ACS Biomaterials SCIENCE & ENGINEERING

Article

pubs.acs.org/journal/abseba

Design and 3D Printing of Hydrogel Scaffolds with Fractal Geometries

John Warner,[†] Pranav Soman,[†] Wei Zhu, Matthew Tom, and Shaochen Chen*

Department of NanoEngineering, University of California, San Diego, 9500 Gilman Drive, La Jolla, California 92093, United States

Supporting Information

ABSTRACT: Structures that exhibit fractal geometries are typically self-similar and iterative. Fractal patterns appear in nature as approximations of mathematical abstractions, yet exist as artifacts of specific processes having reached optimized conditions in the presence of various forces and movements. In this paper, we focus on 3D printing of fractal geometry using computer designed and user adjusted patterns. Various biocompatible hydrogel structures were printed from a photopolymerizable poly(ethylene glycol) diacrylate via maskless stereolithography. This digital micromirror device-based projection printing platform is capable of imbuing fractal topographic patterns into a more cell accommodating medium. Several fractal structures were printed mimicking the energy and material pattern optimization achieved by fractal geometries found in nature. The resulting structures were confirmed with bright-field and SEM microscopy. Complex geometries were obtained at many angles, and various heights that exhibited self-similar geometries. The surfaces of the hydrogel structures were conjugated with fibronectin cell adhesion protein and then seeded with cells. Fluorescent staining of actin and nuclei for both murine myoblast cells and human mesenchymal stem cells were conducted to determine the feasibility of these designed cell adhesive topographies to influence aggregate cells. This flexible and versatile platform can be extended to fabricate other complex biomimetic designs for biological applications, such as tissue engineering.

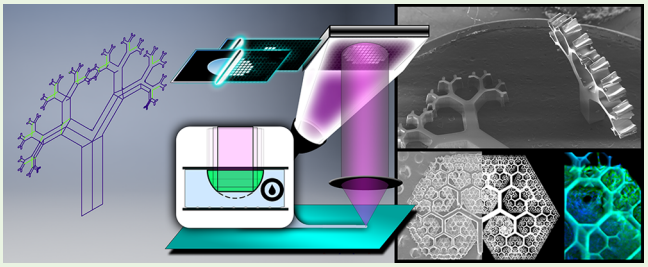

KEYWORDS: *3D printing, hydrogel, fractal, DMD, DOPsL*

INTRODUCTION

Fractal geometry structures are typically iterative self-similar patterns.[1,2] Fractal patterns in nature are artifacts of conditions reached during specific processes that represent useful optimization when organizing materials with regards to forces within a specific medium.[3,4] Such natural optimization can be found in the bifurcation of lungs,[4−8] wild-type and cancerous pulsatile vasculature networks,[3,8−11] the columnar packing of the liver,[12] and the packing of the seeds in sunflowers and pineapples.[13,14] With the ubiquitous existence of fractal patterns in nature, there has been great interest in the bioengineering field to engineer and utilize fractal patterns to study biological questions, such as identifying diseased afflicted cell growth,[9−11] screening cells,[6,10,15,16] and investigating cell proliferation behaviors.[17,18]

Several manufacturing methods have been used to fabricate different designs of engineered fractal scaffolds, including freeze-drying,[19,20] salt leaching,[21,22] electrospinning,[20,23] and fiber deposition.[20,22] Most of these approaches are limited to the overall control of the bulk property of the scaffold and lack the flexibility to tune the fractal design regionally and precisely. The resulting geometries from many of these conventional manufacturing methods are typically fibrous in nature, and "randomly" organized. These primary characteristics emphasize a "roughened" surface area that improves cell growth[7,16,24] and explains the continued use in bioapplications. However, to fabricate geometries with precise control, micro- and nano-manufacturing approaches, such as photolithography,[3,7,25,26] inkjet printing,[20] laser sintering,[27−31] and fused deposition,[3,7,22] have been used instead. However, these manufacturing techniques have limitations in resolution, speed or 3D fabrication capability. Highly complex fractal structures involving large scales can be time-consuming to fabricate with these precision manufacturing methods.

The digital micromirror device (DMD) based projection printing emerges as a high-throughput 3D micro/nano manufacturing technique, offering micrometer resolution, superior fabrication speed[32,33] and a high degree of pattern flexibility[34] and scalability. Recently, we have demonstrated a dynamic optical projection stereolithography (DOPsL) method for printing complex 3D microarchitectures[35] with various photopolymerizable materials such as poly(ethylene glycol) diacrylate (PEGDA), glycidal methacrylate-hyaluronic acid, and gelatin methacrylate.[28,36] These printed hydrogels have shown great biocompatibility for cell seeding and encapsulation.[37]

Special Issue: 3D Bioprinting

Received: March 10, 2016
Accepted: May 23, 2016
Published: May 23, 2016

DOI: 10.1021/acsbiomaterials.6b00140
ACS Biomater. Sci. Eng. 2016, 2, 1763−1770

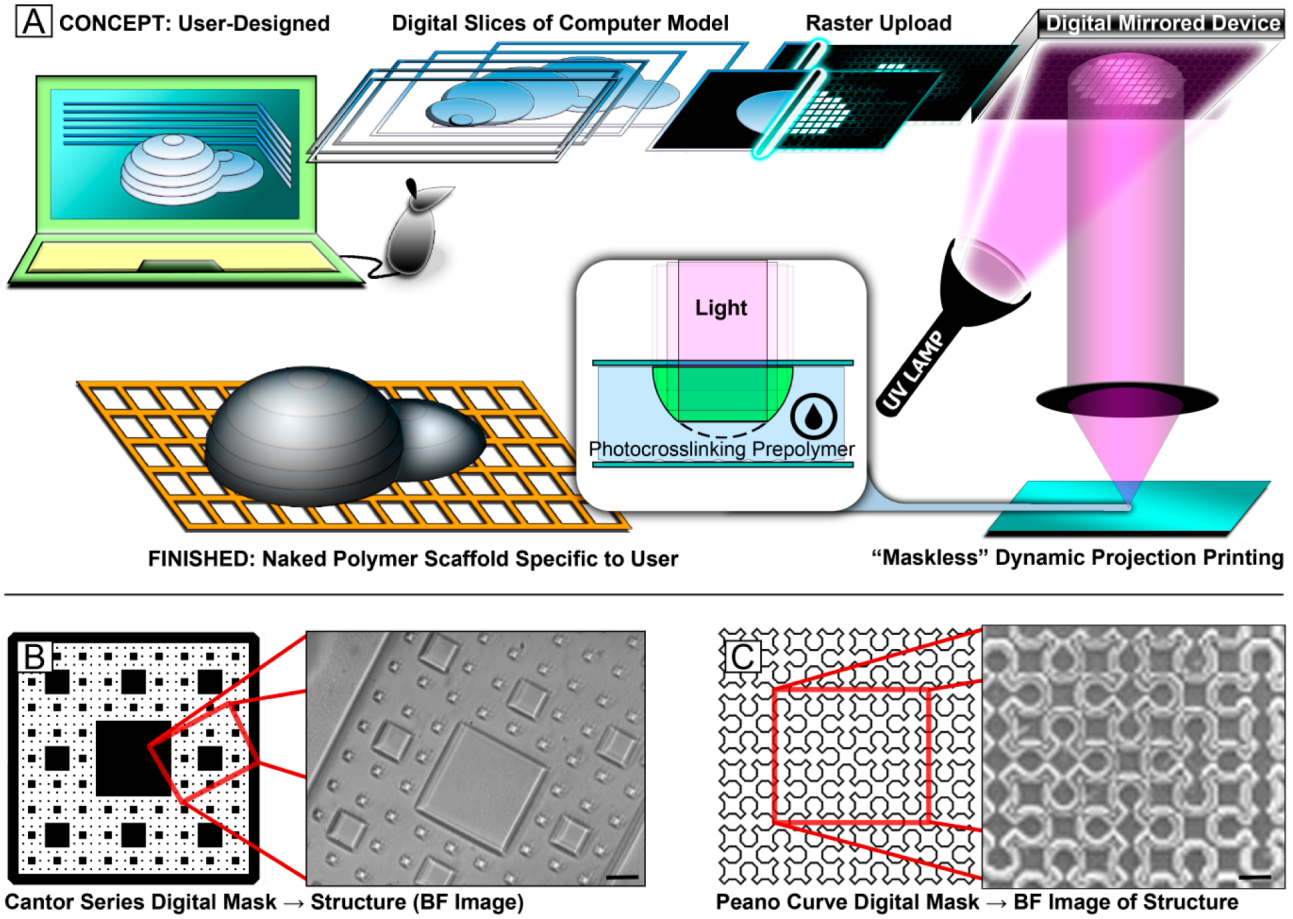

Figure 1. (A) Schematic of the DOPsL system: UV light illuminates the DMD mirror array, which generates an optical pattern according to the images from the control computer. The optical pattern is projected through the optical lens and onto the photosensitive biomaterial to fabricate a 3D scaffold. Simple and complex masks can be used to fabricate fractal scaffolds in a variety of photocurable biomaterials. (B, C) Digital masks (.bmp or .png) and corresponding bright-field microscope images of the Sierpinski carpet and Peano curve fractal geometries fabricated in PEGDA biomaterial. Fabrication settings: (B) Power = 1.3 W/cm^2, exposure time 12 ± 2 s. A narrowed aperture was used to help taper smaller area squares to lower height. (C) P = 1.3 W/cm^2, t = 8 ± 2 s (scale bar = 100 μm).

Here we report the development and application of the DOPsL platform to engineer biomimicking and user-defined fractal patterns. 3D hydrogel structures were printed according to simple mathematical models and complex biomimetic fractal designs. Various structures composed of channels and ridges of varying height and width were printed for the biomimetic fractal patterns. Murine myoblast cells were seeded on the printed fractal scaffolds to demonstrate the biocompatibility of these printed fractal scaffolds in the biological studies. With the superior flexibility and versatility of the DOPsL platform, we were able to fabricate closely packed fractal structures featuring highly complex designs.

EXPERIMENTAL SECTION

Material Preparation. Acrylic acid, 5-benzoyl-4-hydroxy-2-methoxybenzenesulfonic acid (HMBS), poly(ethylene glycol) diacrylate (PEGDA, Mn = 575), and 2,2,6,6-tetramethylpiperdine 1-oxyl (TEMPO) were purchased from Sigma-Aldrich. High purity water was produced by an in-house Millipore system with a resistivity reading 18.2 MΩ upon collection. Irgacure 651, Irgacure 819 and Irgacure 2959 were purchased from Ciba Chemistry. These compounds are photoinitiators generating chemical free radicals when exposed to ultraviolet (UV) light. The solubility of Irgacure 651 is suitable for 100% PEGDA solution, while Irgacure 2959 is suitable for 50% PEGDA in water solution. Irgacure 819 is soluble in 100% PEGDA and has an optical profile more comparable to the UV light source used, despite being more reactive to ambient light. TEMPO mitigates free radical migration distance thus reducing structure bleeding while creating higher aspect ratio structures. HMBS absorbs UV light and increases a gradient against UV light penetration into the structure, providing a better means to control structure height. Acrylic acid polymerizes into the acrylate polymerization chain, anchoring carboxylate functional groups for later chemical conjugation to a peptide. For the 50% PEGDA in water solution, equal volumes of PEGDA and Milli-Q water were mixed in a glass container protected from light. TEMPO [0.01% w/v], HMBS [0.1% w/v], acrylic acid [1.0% v/v], and Irgacure 2959 [1.0% w/v] were added to the solution. The mixture was stirred with a magnetic bar while heated to 60 °C for 1−3 h. The resulting 50% PEGDA solution was used to fabricate the structures presented in Figures 1, 2, 4, and 5A. Figure 3 was printed with TEMPO [0.01% w/v], HMBS [0.1% w/v], and Irgacure 819 [1.0% w/v] to demonstrate z control of the increased polymerization penetration. For the final 100% PEGDA solution, Irgacure 651 [2.00% w/v] and TEMPO [0.04% w/v] were added to PEGDA. The resulting 100% PEGDA was used to fabricate the structure presented in Figure 4B.

DOPsL System Setup. Figure 1A shows the laboratory built DOPsL system used for fabrication of hydrogel fractal geometries. 3D digital models built with computer-aided design software (Autodesk Inventor/Autodesk AutoCAD), or a simple indexed color map relating height in .png format[38] are converted to 2D bitmap slices (MATLAB) and uploaded to the DMD chipset (1920 × 1080, Discover 4000

DOI: 10.1021/acsbiomaterials.6b00140
ACS Biomater. Sci. Eng. 2016, 2, 1763−1770

digital light processing (DLP), Texas Instruments). This bitmap information is translated to spatially tilt a pattern of micromirrors on the DMD chip. The UV light is reflected by the micromirrors and projected through the condensation optics to a focal point within the stage area. A stage controller (Newport) is used to manage the three-axis stage movement, whereas the UV source light (Omnicure S2000) was directed via a light guide toward the DMD chip at a specific angle to facilitate light reflection through the projection optics to the stage. The Omnicure halogen bulb produces a light spectrum filtered to 320−500 nm. A Newport (model 1918) power meter was used to determine the light intensity (1.3×10^3 mW/cm^2 for polymers prepared with I2959 and I651; 6.5 mW/cm^2 for polymers prepared with I819. Exposure times ranged from 6 to 20 s depending on the aperture of light. The DMD chip, the stage and the UV light source are controlled by a desktop computer. The prepolymer is confined between a coverslip and a slide and can be transitioned through the z dimension as the pattern changes. Additionally, the structure can be removed once printed, rinsed, and printed with another layer of a different prepolymer solution.

Scaffold Functionalization. Available carboxyl groups from the copolymerization of acrylic acid and PEGDA were utilized for amine-carboxyl mediated coupling of fibronectin to the hydrogel scaffold. A solution of 1-ethyl-3-[3-(dimethylamino)propyl] carbodiimide hydrochloride (EDC) [0.15 M] (Thermofisher) and N-hydoxysuccinimide (NHS) [0.12 M] (Thermofisher) was prepared in 2-(morpholino)-ethanesulfonic acid (MES) buffer at pH 5. The hydrogel scaffolds were immediately incubated in the prepared working solution for 2 h. Samples were briefly rinsed with Dulbecco's phosphate-buffered saline (DPBS, pH 7.4, Gibco) and then the excess solution was removed. Fibronectin at a concentration of 1 mg/mL was dispensed on the sample surface and allowed to incubate for 24 h at 4 °C protected from light. The residual fibronectin was rinsed and removed, and the samples were sterilized without solution under a UV lamp for ∼30 min.

Cell Culture and Seeding. The human mesenchymal stem cells (hMSC's) were cultured in growth medium consisting of high glucose DMEM (Gibco), fetal bovine serum (10% v/v) (Hyclone), L-glutamine (1%) (Gibco), and penicillin/streptomycin (50 units/mL) (Gibco). Murine myoblasts C2C12 (ATCC) were cultured in growth medium consisting of high glucose DMEM (Gibco), fetal bovine serum (10% v/v) (Hyclone), and penicillin/streptomycin (50 units/mL) (Gibco). Both cell lines were cultured at 37 °C with CO_2 (5.0%) and passaged prior to reaching confluence. Cells from passage 4−6 were seeded on the fibronectin conjugated hydrogel samples at a seeding density of $\sim 2 \times 10^4$/cm^2 and cultured for 1 week.

Bright-Field Imaging. Primary bright-field imaging was performed with a Leica DMI 6000B microscope. The images in Figure 5 were acquired using the tiling functionality of the Leica DMI 6000B at the 10× objective. All other bright field images were not tiled and scale bars of 100 μm are located in the lower right corner.

Immunofluorescent Staining. After 1 week of culture, immunofluorescent staining was performed on the samples. The samples were first fixed with 4% paraformaldehyde (PFA), diluted from 16% stock PFA, with DPBS (pH 7.4) at room temperature for 10 min. Samples were then washed three times with room temperature DPBS (pH 7.4) for 5 min per wash. Fixed samples were simultaneously blocked and permeabilized with 1% BSA, 0.1% Triton-X100 mixture in DPBS (pH7.4) for 20 min. Each sample was incubated with 300 uL of a mixture of Fluor 488 phallodin (Invitrogen) (0.165 μM) to stain actin and 6-diamidino-2-phenylindole (DAPI) (sigma-aldrich) (0.1 μg/mL) to stain nuclei for 30 min at room temperature protected from light. A Zeiss Observer A1 fluorescence microscope was used to take fluorescent images of the samples.

Scanning Electron Microscopy (SEM). The printed hydrogel structures underwent a gradient solvent transfer in order to reduce chance of fracture and were soaked in increasing concentrations of ethanol for 20 min per 10% incremental increases in concentration until ∼100% was reached. Samples were removed from the 100% ethanol solution and placed in a vacuum chamber at room temperature for 24 h. Samples were then sputter coated with iridium (Figure 3-carbon) and imaged via a field-emission environmental microscope (FEI XL30 ESEM FEG). Images were acquired in scattering mode at 10 kV.

RESULTS AND DISCUSSION

We used digital dynamic masks adapted from user-defined computer designed images to fabricate microscale geometries which can be extended to multiple centimeters when the pattern is tile printed (Figure 1A). The DOPsL method uses spatially modulated ultraviolet light to polymerize a liquid prepolymer into a solid 3D structure.[20,27,32,34,39] In essence the DMD chip is an array of reflective coated aluminum micromirrors, capable of creating patterns of light in fast succession, similar to displaying HD (high definition 1920 × 1080) video by controlling each micromirror state as being either "ON' or 'OFF". Regions in the "ON" state are photopolymerized, whereas in the "OFF" state, the pixel appears dark because the illuminated light is reflected away from the condensing projection lens. The micromirror pattern provides a dynamic photomask that can be modified continuously while the reservoir containing the prepolymer solution is translated through the focal plane of the projected image. The prepolymer solidifies in a layer-by-layer fashion as per the user defined digital masks.

Digital masks of typical nonbiological vector-based, space filling fractal patterns (Serpinski carpet, Peano curve) were used to fabricate fractal scaffolds in PEGDA (Figure 1B, C). These patterns were chosen to examine DOPsL printing capabilities of a simple structure scaling over a large dynamic size range, and an extended single ridge fabrication without lateral stabilization from line intersection (normally found in grid designs). The Serpinski carpet pattern, a widely used Cantor series fractal abstraction in mathematics, can be generated by dividing a large square into nine equal smaller squares, removing the central smaller square and reiterating this process a finite number of times. Despite being a purely mathematical abstraction, this structure retains self-similar objects at multiple scales. This scaling property has shown use in screening cell interactions at different scales.[7,15] This could be envisioned as an assembly of different size houses used to determine occupant preferences. The Peano curve is another variation of a space-filling curve[40] that provides increased surface area topography with contortion of a single loop or ridge (Figure 1C). Increased surface area has been used by other groups to facilitate better cell adhesion and faster growth.[7,16,19,24]

PEGDA was used to build these nonbiological patterns to provide an appropriate framework to create representative biological patterns to be extended to relevant biological applications. PEGDA is a synthetic nondegrading water containing gel (hydrogel). This material is considered to be biocompatible, easy to modify, and safe for use in humans. PEGDA can be readily conjugated with peptide adhesion motifs or coated with a physisorbed layer of fibronectin to promote cell adhesion. The mechanical properties of the polymerized PEGDA hydrogel that have been shown to influence cell proliferation and differentiation, such as stiffness and swelling, can also be tuned by the monomer weight, the concentration of the PEGDA monomer or the fabrication parameters (e.g., UV light exposure, time and intensity). This material flexibility provides a chemical means to tune biological patterns for biological use.

DOI: 10.1021/acsbiomaterials.6b00140
ACS Biomater. Sci. Eng. 2016, 2, 1763−1770

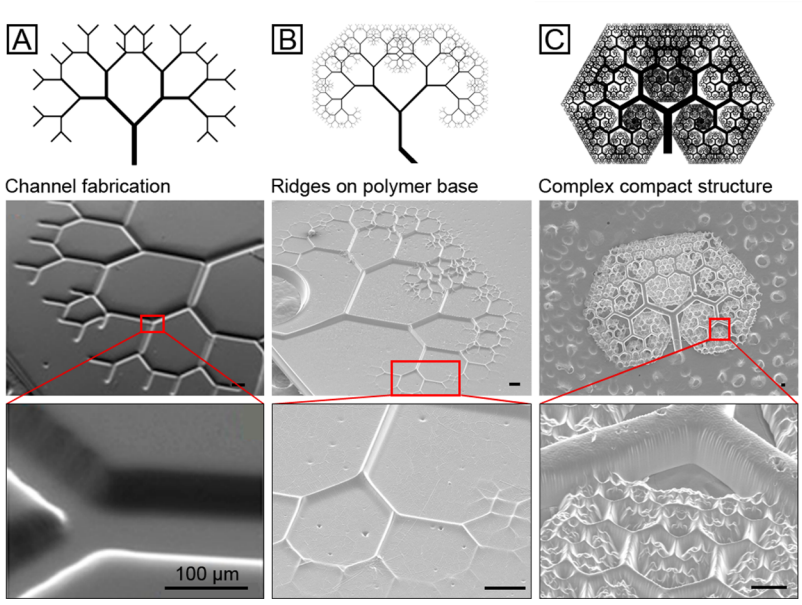

Figure 2. Digital masks of variations of fractal tree patterns. (A, B) SEM images of the A45 R62 tree (a basic bifurcation tree focusing on this ratio 1.618) demonstrate valleys and ridges using inverse masks. (C) SEM image of A60 R75.4 tree representing dimensions of the Pardovan sequence. Fabrication settings: (A) Power: 1.3 W/cm^2, exposure time 8 ± 2 s. (B) P = 1.3 W/cm^2, t = 15 ± 2 s. (C) P = 1.3 W/cm^2, t = 15 ± 4 s. (Scale bar =100 μm).

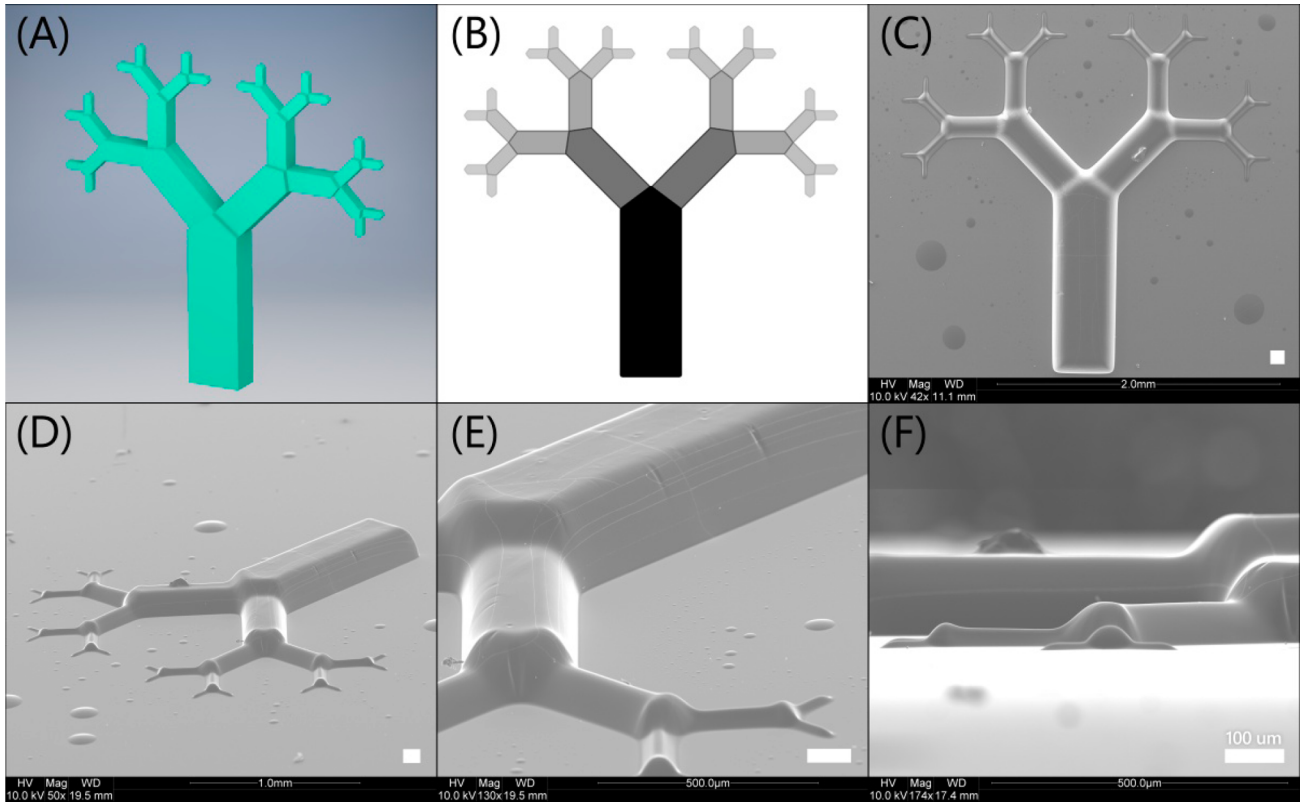

Figure 3. (A) 3D digital tree pattern with linear step profile, (B) corresponding stack of digital masks after applying square function correction to create linear steps (black regions represent mirrors that are "on" longest), (C−F) SEM images of fabricated 100% PEGDA hydrogel coated with carbon on methacrylated glass slide at various viewing angles and magnifications to determine printing fidelity. Fabrication settings: power, 6.5 mW/cm^2; exposure time, 10 ± 1 s. Note: 1.0% Irgacure 819 (photoinitiator) was intentionally chosen to achieve excessive penetration depths, in order to demonstrate z control by only generating a 250 μm structure within a 1 mm prepolymer volume, despite reactivity to ambient light (scale bar = 100 μm).

After demonstrating the ability to pattern more contrived mathematical patterns that explore scalable self-similarity and increased surface area through subdivision of space, we also developed several variations of the fractal tree digital masks to

DOI: 10.1021/acsbiomaterials.6b00140
ACS Biomater. Sci. Eng. 2016, 2, 1763−1770

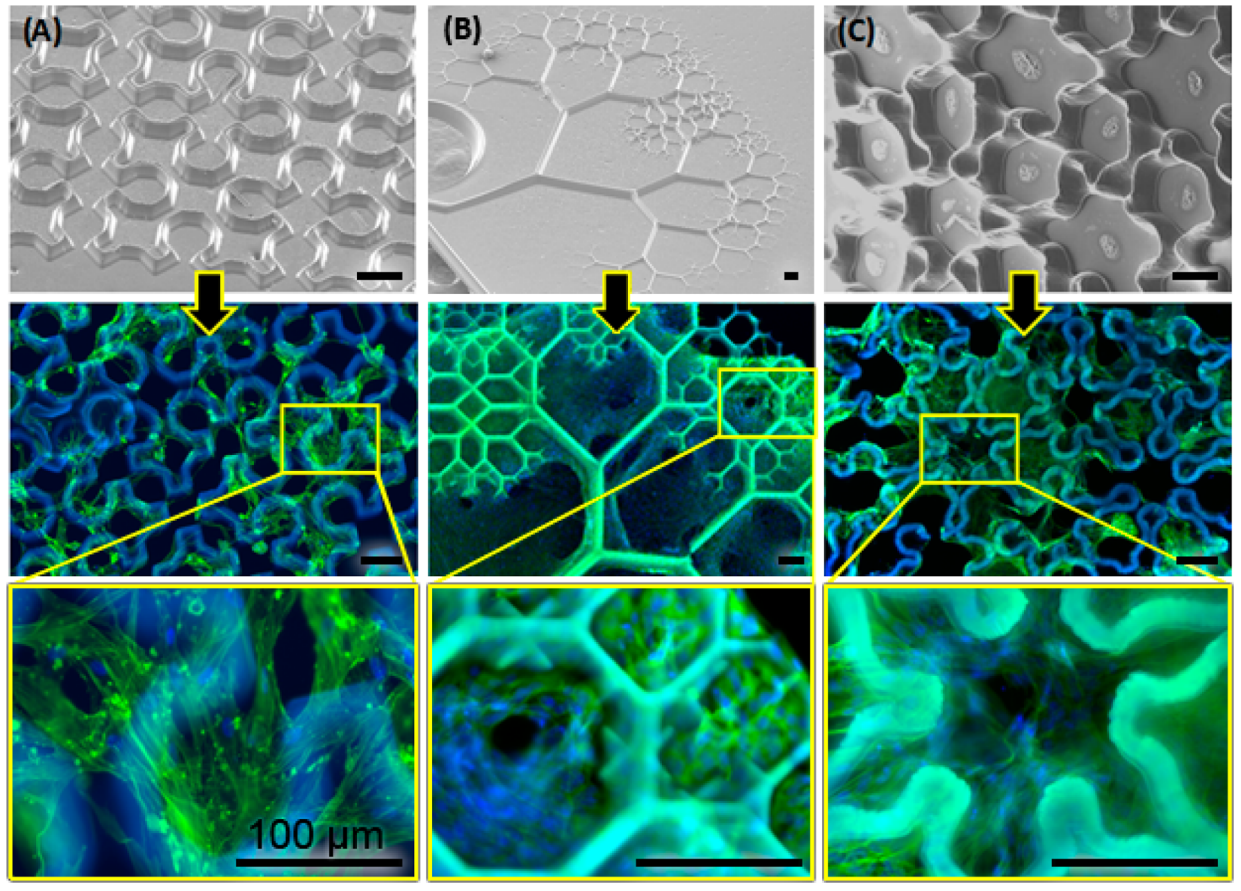

Figure 4. Cell interactions with fractal topographies. (Top row) SEM images of the corresponding hydrogel structures conjugated with fibronectin. (Middle row) fluorescent microscope images taken with 10×:5×:10× (A:B:C) objective DAPI/actin stain. (Bottom row) fluorescent microscope images taken with 40× objective DAPI/actin stain. (A) murine myoblasts (B, C) human mesenchymal stem cells. Fabrication settings: (A) see Figure 1C; (B) see Figure 2B; (C) P = 1.3 W/cm^2, exposure time: 9 ± 2 s on glass (scale bar = 100 μm).

unify these concepts into a synthetic yet more organic or biological looking pattern. The trees (Figure 2) comprise elongated rectangles that in this case bifurcate (divide in two) at angles deviating from the center-line of the previous iteration. These two new rectangles are reduced in dimension compared to the previous rectangle iteration by the indicated ratio. This is a simple synthetic fractal tree that encompasses a bifurcating morphology to more closely mimic the natural formation of branching biological structures. Lungs are organized based on scaling laws to maximize surface area with a volume. When we approximate this to a flattened organ, we look for patterns that effectively fill space (Figure 4). One such ratio is the classic Fibonacci ratio "golden ratio".[4] This ratio arises from the rate of growth found in later elements of the Fibonacci sequence (the sum of the two previous consecutive elements is equal to the value of the next element, where values are integers). This ratio is reported as, φ = 1.618 or 1/0.618, which is significant as being an efficient use of building materials when trying to enclose a growing area with basic squares and claimed to be found in some biological systems. The normally associated 90° angle and the ratio φ have been decoupled as an example of design flexibility to potentially isolate other aspects important to this ratio. Figure 2A shows the A45 R62 (angle 45/ratio 0.62) tree template and the SEM images of fabricated branching channels featuring the fractal tree design with uniform depth (~50 μm). Fabrication of fractal structures in channels shows application in optimizing fluid flow, surface area to volume diffusion, and even pulsatile flows.[4,5,7,39,40] These patterns could also be used as molds for lab-on-chip applications.[41]

Figure 2B demonstrates the fabrication of an A45 R62 fractal tree design with more iterations at higher resolution. Instead of channels, ridges of the fractal tree were printed to show the flexibility of the DOPsL platform. More importantly, this structure is fabricated within one exposure and features ridges stepping down at sequential iterations though narrowing the aperture. This is a unique advantage of DOPsL compared to a conventional photolithography method, where it takes multiple process steps to prepare structures of variable heights.

Figure 2C further extends the complexity of synthetic biomimicking fractal tree designs and fills the empty spaces among the branches with iterating subtrees. The Pardovan ratio (75.4) at 60° was selected as the scaling ratio between the consecutive iterations with a less acute spiral angle that more closely reflects hexagonal packing order of tissue within a layer (e.g., liver), and refines the amount of space-filling in the compact tissue. Variations in design can be developed by changing the degree of branching at each level, branch angle, branch width (pixel width) etc. to develop a library of fractal tree patterns to compare to other similar fractal assemblies. As such, this DOPsL platform is sufficient to create iterations across its scale regime to create hydrogel patterns mimicking many observed natural patterns.

DOI: 10.1021/acsbiomaterials.6b00140
ACS Biomater. Sci. Eng. 2016, 2, 1763−1770

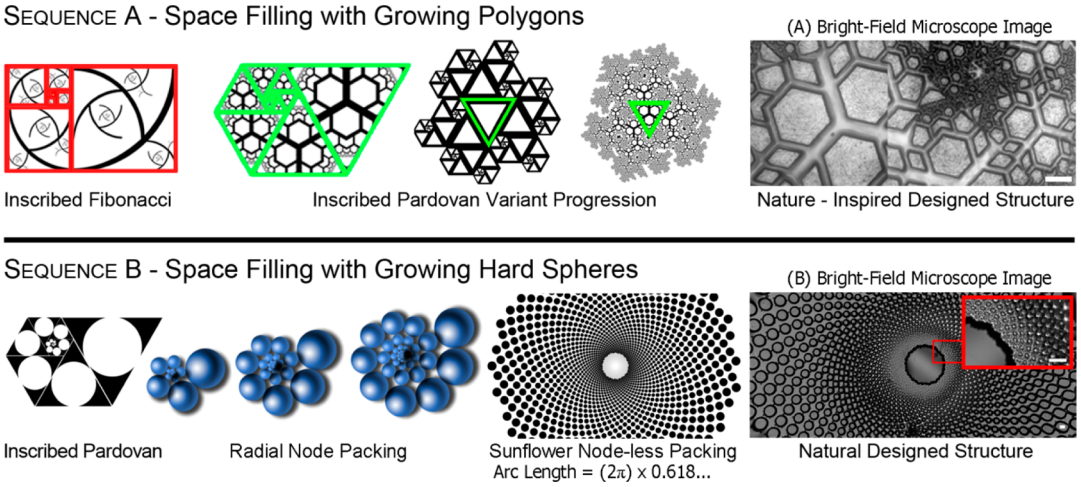

Figure 5. Several compaction models are developed to fill the space optimally. Sequence A: Evolution of simple synthetic fractal design. Fractal patterned tiles substituted or inscribed within solid tiles for generation of more complex structures. The original pattern is translocated, scaled, and repeated to generate organic structures that resemble broccoli heads or pine cones. Image A: The bright-field microscopy image of a printed hydrogel structure from the designed synthetic template. Sequence B: Packing models inscribing growing circles into Pardov's ratio not filling space. A simple hard sphere model showing radial alignment of spheres, also showing gaps in packing structure. Natural "sunflower" design to show more ideal node-less packing of a growing spiral system. The printed "sunflower" design in 100% PEGDA (INSET: detail is maintained close to center) Fabrication Settings: (A) Power: 1.3 W/cm^2, exposure time: 18 ± 2 s; (B) P = 1.3 W/cm^2, t = 16 ± 2 s; sidewall ratio is 6.5 to 1 (scale bar = 100 μm).

Though spine (apex) construction was demonstrated in Figure 2B, linear step control in the z dimension is important in precisely controlling relative height and volume. The following linear stepped structure was printed to better illustrate the DOPsL's printing fidelity which may be determined when comparing the 3D model in Figure 3A to the SEM images in Figure 3C−F. This following structure was created in a 1 mm tall volume of solution despite only being 250 μm in height to demonstrate height control without exterior confinement. The 3D structure slices which make up the digital masks had a function algorithm applied to adjust for light intensity changes over distance in order to create relatively linear step intervals. Figure 3B represents a z-stacked summation of these planar slice masks after applying the algorithm exposure shift. Figures 3C−F show the carbon-coated fractal structure on glass at different angles. The SEM drying process causes some contraction more noticeable at the top of structure, and is evident in corner rounding. Although gradient slopes present little difficultly as seen in our laboratory's previous work,[38] truly vertical sidewalls are difficult to achieve when using soft polymer compositions of HMBS without increasing TEMPO. Vertical sidewalls under high concentrations of TEMPO are presented in the Supporting Information. This structure in Figure 3 presents a scaling fractal tree at user controlled heights decoupled from the length/width ratio to emphasis parametric tunability and printing fidelity of this synthetic branch pattern.

The scaffolds from the previous sections of mathematically abstract patterns (Figure 1C), to synthetic branching patterns (Figure 2B), and more organic hexagonal packing patterns were printed with a biocompatible polymer (PEGDA) and coated with the cell adhesive protein (fibronectin) to demonstrate the potential of 3D-printed scaffolds toward use in bioengineering. Figure 4 shows images of human mesenchymal stem cells (hMSCs) and murine myoblasts seeded on fractal structures made of PEDGA. In this case the PEDGA scaffolds from Figures 1C and 2B were coated with fibronectin, and cells were seeded (passage 4) and stained for actin fibers (phallodin 488/green) and nucleus (DAPI/blue). Figure 4A shows the seeding of murine myoblasts on the Peano curve to effectively increase surface area and shows a cluster of murine myoblasts interacting with the printed curve structures. Figure 4B shows the seeding of hMSCs on the fractal tree design. The cells appear to show some direction bias related to the largest ridge topography, which is inconsistent across varying ridge heights. The magnified region of interest of Figure 4B shows a region of intersecting pattern overlap at the exterior edge. This region contains an area of moderate aspect ridges in close proximity to the single pixel topographies. The cells appear localized near the higher aspect ridges and filling these high-sided wells or gaps, whereas the cells appear to have grown over many of the smaller features, which may provide increased surfaces for binding. Figure 4C shows the seeding of hMSCs on a hexagonal packing structure designed to reflect motifs of compacted cell clusters. More cells were observed spanning across the larger gaps; however, this structure is on a glass substrate which may be influencing this cell behavior. The hydrogel structure was shown as sufficiently biocompatible to murine fibroblast 10T1/2's (Supporting Information). Both cell types were found to adhere and grow on the fractal geometry scaffolds. These results establish the feasibility of using fractal design for addressing biological questions.[41,42]

Moving beyond simple geometries, several compact ordering models can be used as demonstrated in Figure 5. These ratios for compact organization start with classic regular polygon growth systems in the form of Fibonacci and Pardov spirals. Starting from the center and moving to the periphery, these sequences produce enclosed areas at each iteration, and generate new area extension with lower resource cost by utilizing the neighboring "wall" of preexisting structures as seen in all compact spirals. This means that the entire structure as a whole can extend and grow, whereas the existing structure remains completely intact and functional (less vulnerable) during this period. Additionally, the system is compartmentalized, which improves robustness. These are two trends that are advantages to many systems including biological organisms. These basic structures can be inscribed with fractal patterns to

DOI: 10.1021/acsbiomaterials.6b00140
ACS Biomater. Sci. Eng. 2016, 2, 1763−1770

improve surface area as shown in Figure 5A, and carried onto increasingly complex generations via computer, and then printed as shown in the bright field image (Figure 5A). This is an exercise demonstrating user-controlled complexities meshed with known optimizations of a packing order.

This application is more clearly relevant, if we assume our structures of interest are spheres, or have circular footprints which find a packing shape as columnar structures. These columnar growth units become irregular polygonal prisms or hexagonal prism structures[12] when regularly packed as seen with bee honeycombs and liver tissue. However, when we imbue Fibonacci sequence or a Padovan sequence ratio space filling models with inscribed circles we have some gaps as in Figure 4B. A simple model can be used to generate a radial aligned hard sphere packing approximation that can be applied to irregular polygons. This works for some shell structures, however tends to extend these structures farther into the z with volume. We can extend the Fibonacci A + B = A′ Boolean to wrap structures around a circle to achieve the patterns associated with sunflower seeds and pineapples.[13] This classic pattern of seed packing has been well-studied and is noted for having an emanating growth center. Implementing such biomimicry, we can borrow this pattern from nature to create our own hydrogel pattern for "sunflower" node-less packing. This sunflower pattern was fabricated with PEGDA on a slab (Figure 5B). Many natural observed growth patterns deviate from the purely mathematical abstractions and DOPsL platform can accommodate building such structures.

However, because of the minimal cross-sectional area from the design complexity, and lacking structural support due to the soft hydrogel material used, this approach is typically more applicable for complex flatter structures with height and depth but without overhanging ledges. From a manufacturing point-of-view, the advantage of manipulating the fractal dimension through control of surface fractality is very appealing when available during the onset of a design. This control is the primary driving force behind developing algorithm based topographies. Using this algorithm approach, self-similar fractal topographies such as vascular trees based on Lindenmayer models (Pardovan series) or based on Murray's bifurcation laws, can be obtained. Computer implementation to design such patterns also allows parametric design, and a multitude of variations in a design that can be carried out by changing the value of one parameter (for example, the angle, ratio, number of bifurcations, or a fluidic port addition, refer to Figure 5).[43,44] Incorporation of tunable fractality at a design-stage using 3D printing approaches to print structure and localize cells will improve the capabilities of current tissue engineering strategies.[45]

CONCLUSION

We have demonstrated the capabilities of the DOPsL platform as a flexible method to create various fractal forms in a medium conducive to cell growth. Fractal patterns that are purely mathematical, biologically inspired, and directly mimicking observed biological organization have been translated to biocompatible hydrogel photopolymer scaffolds. These moderately complex topographic patterns were implemented as channels or ridges of varying width and height and affect cell alignment as compared to a 2D slab. These results show the topographic possibilities of engineered surface structures to increase surface area, subdivide space in self-similar organization, and produce scaling structures reflecting compact growth. These topographies may have more immediate use in screening "scale" dependent characteristics of cells; however, the goal of imposing optimized biological growth topographies in order to effectively organize cells is still desired. There are many natural systems, and thus many optimized structures to be created. With increasingly accurate computer models of forces, viscosity, diffusion, and aggregation, generating relevant scaffolds for each system is likely possible with the DOPsL platform.

ASSOCIATED CONTENT

Supporting Information

The Supporting Information is available free of charge on the ACS Publications website at DOI: 10.1021/acsbiomaterials.6b00140.

High-aspect-ratio hydrogel sidewall structure: hydrogel structure fabricated at high TEMPO concentration without HMBS to demonstrate nearly vertical sidewalls; printed hydrogel cell viability: fluorescent microscope image of a LIVE/DEAD staining of murine fibroblasts (10T1/2 from ATCC) seeded on fibronectin-conjugated PEGDA photopolymerized hydrogel at day 5 (PDF)

AUTHOR INFORMATION

Corresponding Author

*E-mail: chen168@eng.ucsd.edu.

Author Contributions

†J.W. and P.S. are co-contributor first authors of this work.

Notes

The authors declare no competing financial interest.

ACKNOWLEDGMENTS

The project described was supported in part by the Department of Defense (W81XWH-14-1-0522), California Institute for Regenerative Medicine (RT3-07899) and National Science Foundation (CMMI-1332681 and CMMI-1547005). We thank Dr. Shyni Varghese for kindly providing the MSCs and murine myoblasts and some microscope use for this work. We thank the UCSD Nanoengineering Materials Research Center for SEM imaging. We also thank Peter Chung, Adam H. Aitkenhead, Justin Liu, Xuanyi Ma, and Dr. Donald Sirbuly for their assistance.

REFERENCES

(1) Falconer, K. Fractal Geometry: Mathematical Foundations and Applications. *Biometrics* **1990**, *46*, 886.

(2) Mandelbrot, B. B. The Fractal Geometry of Nature. *Am. J. Phys.* **1983**, *51*, 286.

(3) Yasar, O.; Lan, S.-F.; Starly, B. A Lindenmayer system-based approach for the design of nutrient delivery networks in tissue constructs. *Biofabrication* **2009**, *1* (1), 45004−45009.

(4) Bennett, S. H.; Bennett, S. H.; Eldridge, M. W.; Eldridge, M. W.; Puente, C. E.; Puente, C. E.; Riedi, R. H.; Riedi, R. H.; Nelson, T. R.; Nelson, T. R.; et al. Origin of fractal branching complexity in the lung. Preprint **2000**, available at http://www.stat.rice.edu/~riedi/UCDavisHemoglobin/fractal3.pdf.

(5) Nelson, T. R.; West, B. J.; Goldberger, A. L. The fractal lung: universal and species-related scaling patterns. *Experientia* **1990**, *46* (3), 251−254.

(6) Chen, H.; Gheorgiu, S.; Coppins, M.-O.; Huxley, V. H.; Pfeifer, P.; Krakauer, D.; Tranquillo, R. T.Gas Diffusion through the Fractal Landscape of the Lung: How Deep Does Oxygen Enter the Alveolar System?Losa, G. a., Merlini, D., Nonnenmacher, T. F., Weibel, E. R. In

DOI: 10.1021/acsbiomaterials.6b00140
ACS Biomater. Sci. Eng. 2016, 2, 1763−1770

Fractals in Biology and Medicine; Mathematics and Biosciences in Interaction; Springer: New York, 2005; Vol. *4*, pp 17−30; DOI: 10.1007/3-7643-7412-8.
(7) Vozzi, G.; Previti, A.; Ciaravella, G.; Ahluwalia, A. Microfabricated fractal branching networks. *J. Biomed. Mater. Res.* **2004**, *71* (2), 326−333.
(8) Sun, W.; Darling, A.; Starly, B.; Nam, J. Computer-aided tissue engineering: overview, scope and challenges. *Biotechnol. Appl. Biochem.* **2004**, *39* (1), 29−47.
(9) Cheung, N.; Donaghue, K. C.; Liew, G.; Rogers, S. L.; Wang, J. J.; Lim, S. W.; Jenkins, A. J.; Hsu, W.; Lee, M. L.; Wong, T. Y. Quantitative Assessment of Early Diabetic Retinopathy Using Fractal Analysis. *Diabetes Care* **2009**, *32* (1), 106−110.
(10) Karperien, A.; Jelinek, H. F.; Leandro, J. J. G.; Soares, J. V. B.; Cesar, R. M.; Luckie, A. Automated detection of proliferative retinopathy in clinical practice. *Clin. Ophthalmol.* **2008**, *2* (1), 109.
(11) Masters, B. R. Fractal analysis of the vascular tree in the human retina. *Annu. Rev. Biomed. Eng.* **2004**, *6*, 427−452.
(12) Hayashi, T.; Carthew, R. W. Surface mechanics mediate pattern formation in the developing retina. *Nature* **2004**, *431* (7009), 647−652.
(13) Prusinkiewics, P.; Lindenmayer, A.; Hanan, J.; Fracchia, F.; Fowler, D.; de Boer, M.; Mercer, L. *The Algorithmic Beauty of Plants*; Springer Verlag: Weinheim, Germany, 1996.
(14) Vogel, H. A better way to construct the sunflower head. *Math. Biosci.* **1979**, *44* (3), 179−189.
(15) Unadkat, H. V.; Hulsman, M.; Cornelissen, K.; Papenburg, B. J.; Truckenmüller, R. K.; Carpenter, A. E.; Wessling, M.; Post, G. F.; Uetz, M.; Reinders, M. J. T.; et al. An algorithm-based topographical biomaterials library to instruct cell fate. *Proc. Natl. Acad. Sci. U. S. A.* **2011**, *108* (40), 16565−16570.
(16) Kumar, G.; Waters, M. S.; Farooque, T. M.; Young, M. F.; Simon, C. G. Freeform fabricated scaffolds with roughened struts that enhance both stem cell proliferation and differentiation by controlling cell shape. *Biomaterials* **2012**, *33* (16), 4022−4030.
(17) Eden, M. A two-dimensional growth process. *Berkeley Symp. Math. Stat. Probab.* **1961**, *4*, 223−239.
(18) Ben-Jacob, E.; Schochet, O.; Tenenbaum, a; Cohen, I.; Czirók, a; Vicsek, T. Generic modelling of cooperative growth patterns in bacterial colonies. *Nature* **1994**, *368* (6466), 46−49.
(19) O'Brien, F. J.; Harley, B. A.; Yannas, I. V.; Gibson, L. Influence of freezing rate on pore structure in freeze-dried collagen-GAG scaffolds. *Biomaterials* **2004**, *25* (6), 1077−1086.
(20) Billiet, T.; Vandenhaute, M.; Schelfhout, J.; Van Vlierberghe, S.; Dubruel, P. A review of trends and limitations in hydrogel-rapid prototyping for tissue engineering. *Biomaterials* **2012**, *33* (26), 6020−6041.
(21) Lee, S. B.; Kim, Y. H.; Chong, M. S.; Hong, S. H.; Lee, Y. M. Study of gelatin-containing artificial skin V: Fabrication of gelatin scaffolds using a salt-leaching method. *Biomaterials* **2005**, *26* (14), 1961−1968.
(22) Moroni, L.; De Wijn, J. R.; Van Blitterswijk, C. A. 3D fiber-deposited scaffolds for tissue engineering: Influence of pores geometry and architecture on dynamic mechanical properties. *Biomaterials* **2006**, *27* (7), 974−985.
(23) Zong, X.; Bien, H.; Chung, C. Y.; Yin, L.; Fang, D.; Hsiao, B. S.; Chu, B.; Entcheva, E. Electrospun fine-textured scaffolds for heart tissue constructs. *Biomaterials* **2005**, *26* (26), 5330−5338.
(24) Schwartz Fo, H. O.; Novaes, A. B.; De Castro, L. M. S.; Rosa, A. L.; De Oliveira, P. T. In vitro osteogenesis on a microstructured titanium surface with additional submicron-scale topography. *Clin. Oral Implants Res.* **2007**, *18* (3), 333−344.
(25) Altomare, L.; Gadegaard, N.; Visai, L.; Tanzi, M. C.; Farè, S. Biodegradable microgrooved polymeric surfaces obtained by photolithography for skeletal muscle cell orientation and myotube development. *Acta Biomater.* **2010**, *6* (6), 1948−1957.
(26) Deligkaris, K.; Tadele, T. S.; Olthuis, W.; van den Berg, A. Hydrogel-based devices for biomedical applications. *Sens. Actuators, B* **2010**, *147* (2), 765−774.
(27) Liska, R.; Schuster, M.; Inführ, R.; Turecek, C.; Fritscher, C.; Seidl, B.; Schmidt, V.; Kuna, L.; Haase, A.; Varga, F.; et al. Photopolymers for rapid prototyping. *J. Coatings Technol. Res.* **2007**, *4* (4), 505−510.
(28) Melchels, F. P. W.; Feijen, J.; Grijpma, D. W. A review on stereolithography and its applications in biomedical engineering. *Biomaterials* **2010**, *31* (24), 6121−6130.
(29) Landers, R.; Hübner, U.; Schmelzeisen, R.; Mülhaupt, R. Rapid prototyping of scaffolds derived from thermoreversible hydrogels and tailored for applications in tissue engineering. *Biomaterials* **2002**, *23* (23), 4437−4447.
(30) Tasaki, S.; Maeda, C.; Kirihara, S. *Biofluid Flow Simulation of Tissue Engineering Scaffolds with Dendrite*; Narayan, R., Colombo, P., Eds.; The American Ceramic Society: Westerville, OH, 2013; pp 117−121.
(31) Kumar, G. S.; Pandithevan, P.; Ambatti, A. R. Fractal raster tool paths for layered manufacturing of porous objects. *Virtual Phys. Prototyp.* **2009**, *4* (2), 91−104.
(32) Han, L.-H.; Mapili, G.; Chen, S.; Roy, K. Projection Microfabrication of Three-Dimensional Scaffolds for Tissue Engineering. *J. Manuf. Sci. Eng.* **2008**, *130* (2), 021005.
(33) Sun, C.; Fang, N.; Wu, D. M.; Zhang, X. Projection micro-stereolithography using digital micro-mirror dynamic mask. *Sens. Actuators, A* **2005**, *121* (1), 113−120.
(34) Choi, J. W.; Wicker, R.; Lee, S. H.; Choi, K. H.; Ha, C. S.; Chung, I. Fabrication of 3D biocompatible/biodegradable micro-scaffolds using dynamic mask projection microstereolithography. *J. Mater. Process. Technol.* **2009**, *209* (15−16), 5494−5503.
(35) Zhang, C. A. P.; Qu, X.; Soman, P.; Hribar, K. C.; Lee, J. W.; Chen, S.; He, S. Rapid Fabrication of Complex 3D Extracellular Microenvironments by Dynamic Optical Projection Stereolithography. *Adv. Mater.* **2012**, *24*, 4266−4270.
(36) Ma, X.; Qu, X.; Zhu, W.; Li, Y.-S.; Yuan, S.; Zhang, H.; Liu, J.; Wang, P.; Lai, C. S. E.; Zanella, F.; et al. Deterministically patterned biomimetic human iPSC-derived hepatic model via rapid 3D bioprinting. *Proc. Natl. Acad. Sci. U. S. A.* **2016**, *113*, 2206−2211.
(37) Qu, X.; Zhu, W.; Huang, S.; Li, Y. S.; Chien, S.; Zhang, K.; Chen, S. Relative impact of uniaxial alignment vs. form-induced stress on differentiation of human adipose derived stem cells. *Biomaterials* **2013**, *34* (38), 9812−9818.
(38) Soman, P.; Chung, P. H.; Zhang, A. P.; Chen, S. Digital microfabrication of user-defined 3D microstructures in cell-laden hydrogels. *Biotechnol. Bioeng.* **2013**, *110* (11), 3038−3047.
(39) West, G. B.; Brown, J. H.; Enquist, B. J. A general model for the origin of allometric scaling laws in biology. *Science (Washington, DC, U. S.)* **1997**, *276* (5309), 122−126.
(40) Marxen, M.; Henkelman, R. M. Branching tree model with fractal vascular resistance explains fractal perfusion heterogeneity. *Am. J. Physiol. Heart Circ. Physiol.* **2003**, *284* (5), H1848−H1857.
(41) Liu, J.; Hwang, H. H.; Wang, P.; Whang, G.; Chen, S. Direct 3D Printing of Cell-laden Constructs in Microfluidic Architectures. *Lab Chip* **2016**, *16*, 1430−1438.
(42) Salter, P. S.; Booth, M. J. Addressable microlens array for parallel laser microfabrication. *Opt. Lett.* **2011**, *36* (12), 2302−2304.
(43) Soo, S. C.; Yu, K. M. Rapid prototyping for self-similarity design. *J. Mater. Process. Technol.* **2003**, *139* (1−3), 219−225.
(44) Sun, W.; Lal, P. Recent development on computer aided tissue engineering — a review. *Comput. Methods Programs Biomed.* **2002**, *67* (2), 85−103.
(45) Díaz Lantada, A.; Pareja Sánchez, B.; Gómez Murillo, C.; Urbieta Sotillo, J. Fractals in tissue engineering: toward biomimetic cell-culture matrices, microsystems and microstructured implants. *Expert Rev. Med. Devices* **2013**, *10* (5), 629−648.

DOI: 10.1021/acsbiomaterials.6b00140
ACS Biomater. Sci. Eng. 2016, 2, 1763−1770